Journal of Geosciences, 55 (2010), 231–249 DOI: 10.3190/jgeosci.077

Original paper

Clinopyroxene from basaltic rocks of the Erzgebirge-Krušné hory Mts. – implications for modelling of the magmatic plumbing system

Roman RÖNICK[1], Axel D. RENNO[1*]

[1] *Technische Universität Bergakademie Freiberg, Institute of Mineralogy, Brennhausgasse 14, D-09596 Freiberg, Germany; axel.renno@mineral.tu-freiberg.de*

[*] *Corresponding author*

The Erzgebirge-Krušné hory area is part of the NW flank of the Eger-Ohře Rift. Within this rift-related area, basaltic rocks with low (< 3.5 wt. %) and high contents (> 3.5 wt. %) of TiO_2 occur. The distribution of these basaltic rock types shows strong spatial dependency. Ti-rich basalts are concentrated in the western Erzgebirge-Krušné hory Mts. with a sharp change at longitude 13.3 °E. Clinopyroxene and olivine are the most abundant phenocrysts. The zoning and chemistry of the clinopyroxene act as a recorder of the different stages of the magmatic plumbing systems. Seven different types of clinopyroxene phenocrysts are defined with four distinct chemical types: Cr-rich clinopyroxene, green-core pyroxene, Mg-rich clinopyroxene and finely zoned Ti-rich clinopyroxene with sector zoning.

Chemical and petrographic analysis of individual zones within clinopyroxenes allows the qualitative description of distinct steps of the multistage, regionally diverse processes yielding to the formation of both Ti-rich basalts in the W as well as Ti-poor basalts in the E. Two different types of asthenospheric melts are suggested, with increased activities of H_2O and potassium in the western Erzgebirge Mts. During ascent they incorporated xenoliths and xenocrysts of both the mantle (peridotite, olivine and Cr-rich clinopyroxene) and the crustal (granitic and gneissic rocks, quartz and feldspar) origin. Furthermore, green cores of clinopyroxene were introduced into the magmas. Fractionation processes took place within lithospheric magma chambers, having been accompanied by reaction of xenocrysts and xenoliths with the melt. The residence time in the magma chambers associated with the eastern and western parts of the Erzgebirge appears to have been totally different: short in the eastern and long in the western parts. Within the latter, no mantle-derived xenoliths, xenocrysts, or magmatic olivines are found. It is inferred that these xenoliths and crystals settled to the bottom of the magma chambers forming cumulates and therefore did not come to the surface. In contrast, the basaltic rocks of the East still contain mantle-derived xenoliths and xenocrysts as well as magmatic olivine. The size and amount of clinopyroxene phenocrysts in the West significantly exceed that of the East. Moreover, the crystallization of giant clinopyroxenes was restricted to the western region. Mixing of the magmas with Ti-rich melts, presumably derived from an eclogitic source, took place in crustal magma chambers. In any case, the proportion of Ti-rich melts in the West significantly exceeded that of the East.

Keywords: petrology, crystal chemistry, clinopyroxene, basalt, Erzgebirge-Krušné hory, green-core pyroxene
Received: 6 April 2010; accepted: 20 September 2010; handling editor: V. Rapprich/R. Skála
The online version of this article (doi: 10.3190/jgeosci.077) contains supplementary electronic material.

1. Introduction

Despite the eye-catching geochemical character of '*Ti-rich basalts*' it is unclear if this feature is a vagary of nature or an important geochemical fingerprint able to discriminate between different source regions of basaltic rocks. Besides well known High-Ti basalts from the moon (Papike et al. 1976; Papike and Vaniman 1978), which have no terrestrial equivalent, High-Ti basalts are found in different geotectonic settings, such as Continental Flood Basalts (CFB), Large Igneous Provinces (LIP) (Gibson et al. 1995), or rift-like intraplate settings (Pik et al. 1998). The occurrence of such basalts is not restricted to lavas; they appear also in dike systems (Essawy and El-Metwally 1999; Katzir et al. 2006) and intrusions of gabbroic rocks (Jama Aden and Frizzo 1996). Their age spans from the Archaean to recent. The origin in each of the geotectonic environments remains controversial. The proposed explanations in LIPs range from a high degree of fractionation (Fodor 1987), low degree of partial melting (Dupuy et al. 1988), crustal contamination (Fodor 1987), to the influence of subcontinental lithosphere mobilized by subduction (Duncan 1987; Murphy 1988). It is assumed that the effect of mantle plumes is the main cause for the genesis of Ti-rich rocks in rift-like settings (Pik et al. 2006).

A qualitative approach to understanding petrological processes responsible for the genesis of Ti-rich basalts through the comprehensive study of the microstructure and mineral chemistry of clinopyroxene is demonstrated in the

current paper. As a case study have been chosen Cenozoic basaltic rocks from the Eger-Ohře Rift (Erzgebirge-Krušné hory Mts, Bohemian Massif). Although we do not present a complete genetic model, this study does provide a basis for understanding the nature and genesis of the high-Ti basalts, both in this region and elsewhere.

2. Geological setting

According to Prodehl et al.(1995) the Eger-Ohře Rift, as part of the European Cenozoic Rift System (ECRS), is one of the major extensional structures in Central Europe. The structure itself is situated in Proterozoic to Paleozoic basement rocks of the Bohemian Massif (Malkovský 1987; Mlčoch and Konopásek 2010) and shows an elongation of roughly 300 km and a width up to ~ 30 km. The western part of the Eger Rift lies on a Variscan suture zone between two lithospheric blocks: the Saxothuringian and the Teplá–Barrandian terranes (Hrubcová et al. 2005; Babuška et al. 2007). The thermal thickness of the lithosphere at the level of the 1 300 °C isotherm has been modelled to be 110–170 km, whereas the mechanical thickness is only 65–90 km (Babuška and Plomerová 1992; Goes et al. 2000). Plomerová et al. (2007) with Babuška and Plomerová (this volume) found clear differences in the orientations of seismic anisotropy in the three major tectonic units (Saxothuringian, Moldanubian and Teplá–Barrandian), but no signs for the existence of plume-like structures in the mantle. The region shows evidence for repeated magmatic phases before the Tertiary but most of the Eger Rift lavas erupted between 30 and 15 Ma both within the rift and on its NW flank (Todt and Lippolt 1975; Pilot et al. 1984; Kaiser and Pilot 1986; Ulrych et al. 2002).

The NW-flank of the western part of the Eger Rift lies in the Erzgebirge-Krušné hory Mts. part of the Saxothuringian Zone of the Bohemian Massif, which is known to host volcanic rocks with distinct differences in the TiO_2 contents (Pfeiffer 1978; Niese et al. 1995; Shrbený 1995; Ulrych et al. 2005; Haase and Renno 2008). Detailed studies of the mineral chemistry of clinopyroxene in the basaltic rocks of the Eger Rift are rare so far (Ulrych 1986; Ulrych et al. 1990; Rapprich 2005) and the current manuscript aims to bring new data in this respect.

3. Sampling and methods

The first step of sampling was the verification of all outcrops of basaltic rocks evinced in the 1 : 25 000 geo-

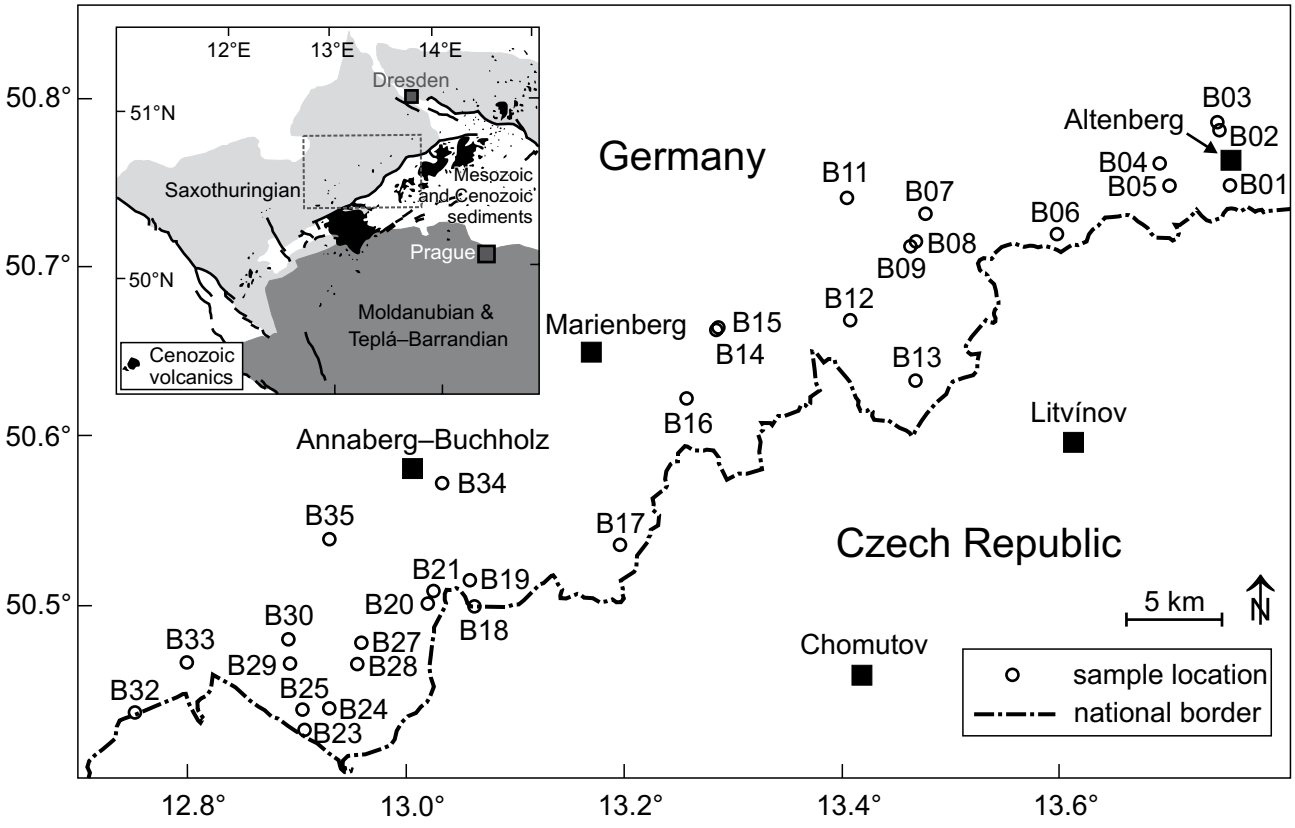

Fig. 1 Location of the samples. The locations, including GPS coordinates, are summarized in Tab. 1.

logical maps of the German part of the Erzgebirge. The eventual sampling covered 27 localities (Tab. 1 and Fig 1). The samples were selected on the basis of the major-element composition, i.e. only primitive rock types were chosen.

Fresh pieces were cut and washed in distilled water and an ultrasonic bath before crushing. The crushed rock sample was milled to powder in an agate ball mill. Whole-rock major-element analyses were measured with a Bruker "Tiger S8" X-ray fluorescence spectrometer at the Institut für Mineralogie, TU Bergakademie Freiberg using rock standards for calibration and quality control.

Mineral analyses were carried out using a JEOL JXA8900 electron microprobe at the Institut für Mineralogie, TU Bergakademie Freiberg. The analytical conditions for the minerals were an accelerating voltage of 15 keV, a beam current of 30 nA and a focused beam. Counting times were 20–50 s for peak and 10–25 s for background positions. An accelerating voltage of 20 keV and a beam current of 40 nA were used for X-ray concentration maps and concentration profiles. Natural mineral standards and the ZAF matrix correction was employed.

All data were visualized using the GCDkit software package (Janoušek et al. 2006).

4. Geochemistry

Representative whole-rock analyses of the lavas are presented in Tab. 1. All the analyzed basaltic rocks represent truly alkali basaltic rocks, mostly basanites and melanephelinites (Supp. 1), according to the total alkali vs. SiO_2 (TAS) classification scheme of Le Bas et al. (1986) and Le Maitre et al. (2005). We stuck to the proposals of Le Bas (1989) and Middlemost (1994) for further discrimination between basanite/tephrite and nephelinite/melanephelinite (Fig. 2).

4.1. Major elements and trace elements

All samples form a continuous trend with decreasing TiO_2, FeO^T, and CaO and increasing MgO, and Al_2O_3 with increasing SiO_2 (Fig. 3a–d and Supp. 2). With rising FeO^T/MgO, ratio, often used as a differentiation index, TiO_2, and CaO show a continuous increase, while Cr, and Ni drop sharply (Fig. 3e and Supp. 2). The lavas show two separate positive trends in binary diagram of FeO^T/MgO vs. Al_2O_3 (Fig. 3f). Some trace elements (e.g. Nb, V, and Zr) are positively correlated with TiO_2 (Fig. 3g and Supp. 2), whereas the ratio CaO/Al_2O_3 shows a clear splitting at *c.* 3.5 wt. % TiO_2 (Fig. 3h).

4.2. Regional variation

A striking feature is the regional dichotomy in whole-rock compositions of basalts from the eastern and western Erzgebirge. At a longitude of 13.3 °E we observed an abrupt change (Supp. 3), best exemplified by TiO_2 (Fig. 4). Despite a small overlap, TiO_2 (threshold value 3.5 wt. %) and CaO (threshold value 13.5 wt. %) drop eastwards, while Al_2O_3 (threshold value 12 wt. %),

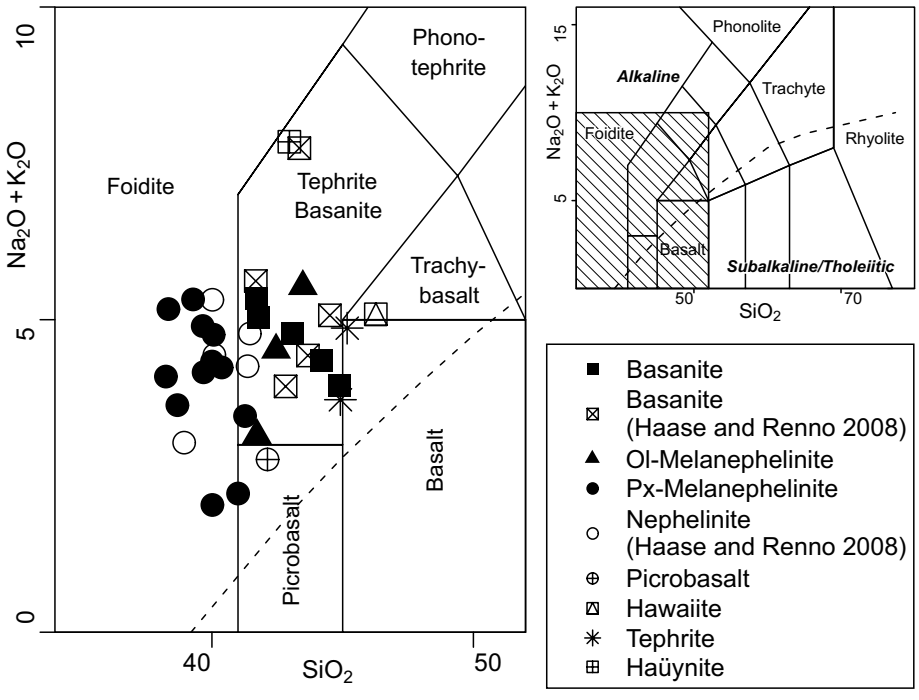

Fig. 2 Total alkali vs. SiO_2 (TAS) diagram for the analysed basaltic rocks and some additional samples from the same area (Haase and Renno 2008).

Tab. 1 Whole-rock major- and trace-element compositions for the studied basaltic rocks from the eastern and western Erzgebirge (Germany)

Sample	**B01**	**B02a**	**B03a**	**B05**	**B06**	**B07**	**B08**
Locality	NNW Zinnwald	SE Hirschsprung	Hirschsprung	road Altenberg–Rehefeld	Steinkuppe near Holzhau	Ziegenberg near Claußnitz	"Kreuztanne"
Latitude °N	50.749	50.782	50.786	50.749	50.720	50.730	50.715
Longitude °E	13.76	13.75	13.75	13.71	13.60	13.47	13.47
Rock type	basanite	basanite	basanite	Ol-Mn	Ol-Mn	Ol-Mn	hawaiite
SiO_2	42.29	40.97	40.71	40.27	42.34	41.75	45.13
TiO_2	2.72	3.71	3.59	3.37	3.14	3.07	3.20
Al_2O_3	12.68	13.72	13.11	12.66	13.44	13.26	13.63
Fe_2O_3t	12.39	13.36	13.27	13.91	12.37	12.92	12.25
MgO	12.17	9.93	10.84	9.99	9.18	10.57	8.80
MnO	0.19	0.19	0.19	0.23	0.20	0.21	0.22
CaO	11.67	11.75	11.46	13.39	11.73	12.74	9.88
Na_2O	3.32	3.75	3.63	2.55	4.25	3.59	3.66
K_2O	1.37	1.49	1.27	0.49	1.13	0.85	1.30
P_2O_5	0.60	0.73	0.71	1.06	0.83	0.68	0.69
L.o.I.	0.23	0.40	0.35	0.88	0.50	0.40	0.46
Total	99.63	100.01	99.13	98.79	99.11	100.03	99.22
B	76	128	134	100	112	97	112
F	491	897	776	252	898	528	869
S	190	270	230	190	260	240	470
Cl	179	250	218	bd	212	bd	bd
V	223	268	261	252	271	254	211
Cr	361	136	188	157	189	290	102
Co	51	46	48	43	41	48	40
Ni	209	108	152	130	110	138	90
Cu	48	61	53	31	38	43	35
Zn	97	97	97	97	97	97	97
Ga	17	18	17	17	18	17	18
As	2	3	3	5	8	4	19
Br	4	4	4	2	4	3	3
Rb	32	53	48	49	39	45	49
Sr	618	710	688	1344	782	701	707
Y	20	21	20	22	23	22	22
Zr	206	236	226	270	264	226	243
Nb	60	68	68	58	71	57	55
Mo	bd	1	4	2	4	2	4
Ag	bd	bd	bd	bd	bd	bd	bd
Cd	bd	bd	bd	bd	1	bd	1
Sn	5	7	5	9	4	6	4
Cs	0.6	2.4	1.2	bd	2.2	5.7	39.8
Ba	434	499	468	707	632	542	668
La	38	52	55	83	76	49	55
Ce	86	90	87	133	125	99	93
Pb	4	5	2	7	bd	4	bd
U	11.2	11.4	11.5	15.6	11.2	11.0	10.2

bd = below detection limit; Mn = melanephelinite

Tab. 1 Continued

Sample	B11b	B12b	B13	B14a	B15	B16	B17
Locality	Galgenberg (road way Voigtsdorf–Sayda)	Schafferholz (Heidersdorf)	Ahornberg (Seiffen)	SW Blumenau	SW Blumenau	Rabenberg (SE Zöblitz)	Hirtstein (N Satzung)
Latitude °N	50.740	50.668	50.632	50.662	50.663	50.622	50.536
Longitude °E	13.40	13.41	13.47	13.28	13.28	13.25	13.19
Rock type	basanite	basalt	basanite	Cpx-Mn	picrobasalt	Cpx-Mn	Cpx-Mn
SiO_2	43.74	47.24	43.63	39.63	41.23	39.23	39.13
TiO_2	2.98	2.72	2.36	3.88	3.83	4.32	4.04
Al_2O_3	12.40	13.48	11.09	10.16	10.30	11.17	10.42
Fe_2O_3t	11.75	11.12	12.01	14.31	14.22	14.94	14.47
MgO	10.53	8.27	16.01	9.07	9.36	8.26	8.85
MnO	0.18	0.18	0.18	0.21	0.20	0.22	0.22
CaO	12.29	11.31	9.66	17.97	16.75	15.54	16.45
Na_2O	2.95	3.12	3.07	1.63	1.91	2.95	2.83
K_2O	0.90	0.99	1.23	0.51	0.80	1.16	1.82
P_2O_5	0.93	0.50	0.70	0.72	0.70	0.86	0.90
L.o.I.	0.51	0.76	0.11	0.94	0.55	0.36	0.56
Total	99.17	99.68	100.06	99.03	99.84	99.01	99.67
B	115	109	88	126	118	146	146
F	505	375	bd	1344	1245	692	1385
S	300	240	110	910	580	300	320
Cl	bd	bd	85	396	170	bd	bd
V	242	237	183	383	371	416	393
Cr	299	272	549	185	193	100	100
Co	43	41	60	46	49	46	49
Ni	136	130	445	56	59	38	50
Cu	50	43	35	197	196	244	283
Zn	97	97	97	97	97	97	97
Ga	17	17	17	17	18	19	18
As	3	7	6	2	5	1	5
Br	3	3	4	4	3	3	3
Rb	38	207	32	58	45	49	43
Sr	768	548	765	701	729	790	804
Y	23	28	18	18	19	23	21
Zr	237	198	221	231	237	280	305
Nb	67	48	69	77	74	96	95
Mo	3	1	1	2	bd	bd	bd
Ag	bd	bd	bd	bd	bd	bd	bd
Cd	bd	bd	bd	bd	bd	bd	bd
Sn	4	6	6	6	6	3	3
Cs	1.5	5.5	0.7	1.7	2.2	bd	bd
Ba	602	867	448	585	898	978	531
La	70	42	55	63	64	84	83
Ce	124	83	125	113	117	148	135
Pb	4	6	5	6	5	3	6
U	11.3	6.0	12.5	10.4	8.1	7.9	11.7

bd = below detection limit; Mn = melanephelinite

Tab. 1 Continued

Sample	**B18c**	**B19**	**B21**	**B24**	**B25**	**B27a**	**B30b**
Locality	SW Jöhstadt (state frontier)	Klöfs–Berg (W Jöhstadt)	Bärenstein (W Bärenstein)	Wurzelbergstraße (Oberwiesenthal)	Einsberg (NE Tellerhäuser)	Morgenberg (W Neudorf)	Eisensteinberg (W Neudorf)
Latitude °N	50.501	50.516	50.508	50.442	50.439	50.479	50.481
Longitude °E	13.06	13.05	13.02	12.93	12.90	12.96	12.89
Rock type	Ol–Cpx-leucitite	Cpx-Mn	Cpx-Mn	tephrite	Cpx-Mn	haüynite	Cpx-Mn
SiO_2	40.79	38.91	38.18	43.74	40.31	41.56	38.76
TiO_2	3.95	4.37	5.02	3.75	4.68	4.12	4.75
Al_2O_3	10.71	10.38	11.04	12.99	11.55	13.79	11.24
Fe_2O_3t	13.89	16.09	16.23	12.92	15.01	12.65	14.74
MgO	10.11	8.31	7.05	6.74	7.26	4.32	8.25
MnO	0.18	0.21	0.27	0.20	0.22	0.28	0.23
CaO	14.81	16.64	14.61	12.42	15.91	12.36	15.58
Na_2O	2.27	2.79	3.93	3.59	2.60	4.20	3.30
K_2O	2.14	1.29	1.25	1.12	0.78	3.39	1.49
P_2O_5	0.62	0.69	1.26	0.65	0.87	1.33	0.88
L.o.I.	0.25	0.27	0.44	0.67	0.63	0.52	0.55
Total	99.72	99.95	99.28	98.79	99.83	98.52	99.76
B	112	146	160	126	162	180	169
F	560	1370	1643	1376	1443	1915	2155
S	330	410	270	1020	390	2100	600
Cl	bd	bd	bd	bd	bd	1517	200
V	369	454	408	324	410	352	393
Cr	270	26	12	62	37	10	88
Co	48	53	45	44	48	27	45
Ni	80	38	28	53	31	11	53
Cu	247	414	82	81	262	31	178
Zn	97	97	112	97	99	131	97
Ga	17	20	21	19	20	25	19
As	4	5	2	7	3	7	4
Br	3	4	3	3	3	7	4
Rb	70	36	40	46	82	77	37
Sr	456	833	899	788	731	1498	829
Y	20	19	27	23	22	38	22
Zr	220	262	377	247	306	523	293
Nb	76	89	107	76	89	157	94
Mo	bd	bd	bd	9	bd	3	bd
Ag	bd	bd	bd	bd	bd	bd	bd
Cd	bd	bd	1	bd	1	bd	bd
Sn	7	4	6	6	8	8	5
Cs	bd	0.6	bd	bd	bd	bd	bd
Ba	1024	697	511	664	439	954	621
La	62	76	108	74	72	148	86
Ce	123	117	169	121	117	260	142
Pb	4	6	bd	7	bd	16	5
U	4.4	10.5	12.9	10.9	11.6	14.4	11.3

bd = below detection limit; Mn = melanephelinite

Tab. 1 Continued

Sample	B30c	B32	B33a	B33b	B34	B35
Locality	Eisensteinberg (W Neudorf)	Glücksburg Berg (E Johanngeorgenstadt	Vordere Kohlung (S Rittersgrün)	Vordere Kohlung (S Rittersgrün)	Pöhlberg (E Annaberg–Buchholz)	Scheibenberg (E Scheibenberg)
Latitude °N	50.481	50.436	50.467	50.467	50.574	50.540
Longitude °E	12.89	12.75	12.80	12.80	13.03	12.92
Rock type	tephrite	Cpx-Mn	Cpx-Mn	Cpx-Mn	Cpx-Mn	Cpx-Mn
SiO_2	43.63	38.94	37.10	39.17	37.20	37.79
TiO_2	4.18	4.81	4.97	4.39	5.03	5.12
Al_2O_3	11.02	10.28	11.42	10.92	11.33	11.03
Fe_2O_3t	12.55	15.29	15.30	15.21	15.74	16.19
MgO	7.98	10.46	6.35	8.25	6.37	7.92
MnO	0.19	0.21	0.25	0.21	0.26	0.22
CaO	14.48	16.13	17.86	16.24	16.11	16.51
Na_2O	2.35	1.50	2.99	2.84	3.65	2.57
K_2O	1.27	0.49	0.98	1.40	1.36	0.98
P_2O_5	0.76	0.75	1.33	0.81	1.56	1.00
L.o.I.	0.77	1.01	0.45	0.34	0.42	0.58
Total	99.17	99.85	99.01	99.77	99.03	99.90
B	155	163	176	155	164	151
F	1734	1734	1671	1446	2466	2034
S	1940	530	960	470	1050	820
Cl	bd	115	bd	bd	425	bd
V	350	389	437	422	464	475
Cr	116	193	10	74	17	49
Co	42	52	44	50	52	54
Ni	60	82	12	39	21	39
Cu	148	213	295	330	186	287
Zn	97	97	104	97	122	106
Ga	17	17	20	19	24	22
As	5	5	4	3	5	5
Br	3	4	3	3	5	4
Rb	77	53	50	44	56	47
Sr	1009	667	998	857	822	807
Y	22	19	25	20	36	31
Zr	253	258	352	270	426	345
Nb	89	68	90	83	114	106
Mo	4	bd	1	bd	bd	2
Ag	bd	bd	bd	bd	2.3	bd
Cd	bd	bd	bd	1	bd	bd
Sn	8	7	6	7	7	6
Cs	0.3	bd	bd	bd	2.8	bd
Ba	662	540	745	903	302	610
La	79	74	95	74	98	89
Ce	135	131	173	136	179	144
Pb	6	5	8	1	12	10
U	12.6	10.4	11.6	9.1	12.9	10.1

bd = below detection limit; Mn = melanephelinite

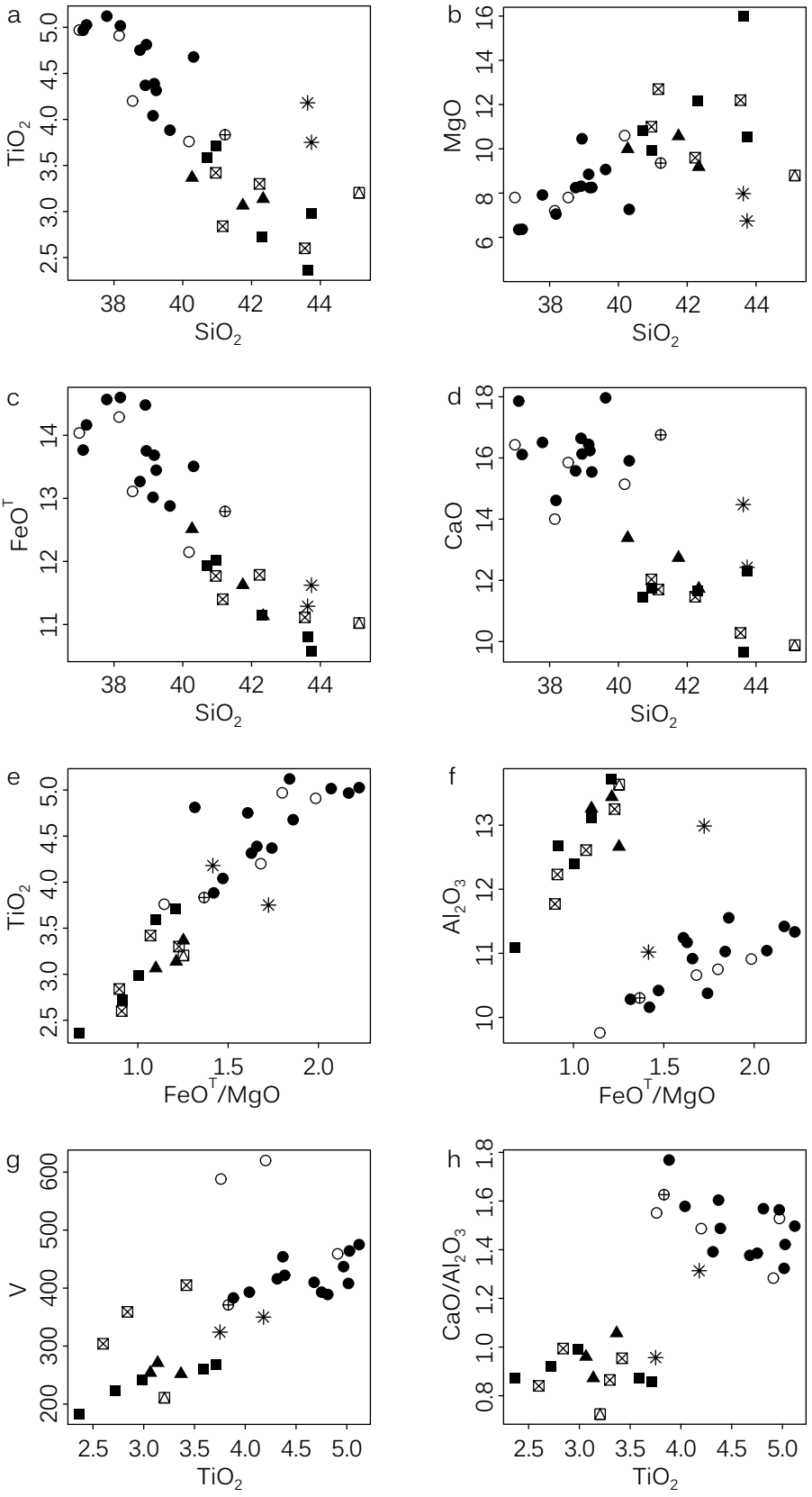

Fig. 3 Selected variation diagrams for the Erzgebirge basaltic rocks. Symbols and additional data sources as in Fig. 2. **a** – SiO_2 vs. TiO_2; **b** – SiO_2 vs. MgO; **c** – SiO_2 vs. FeO^T; **d** – SiO_2 vs. CaO; **e** – FeO^T/MgO vs. TiO_2; **f** – FeO^T/MgO vs. Al_2O_3; **g** – TiO_2 vs. V; **h** – TiO_2 vs. CaO/Al_2O_3.

and mg# (threshold value 58) increase. Such variations are known from other parts of the ECRS like the Vogelsberg (Bogaard and Wörner 2003) and the Rhön (Jung and Hoernes 2000).

5. Petrography

The petrography of all samples was described in detail by Rönick (2010). The main features are compiled in Supp. 1.

5.1. Groundmass

All rocks show a porphyritic microstructure with a fine-grained groundmass. This groundmass consists of small, elongate clinopyroxene and isometric opaque minerals. Some lavas show flow patterns or schlieren-like inhomogeneities. Additionally minerals of the sodalite-group, nepheline, perovskite, and analcime occur, predominantly in the rocks from the western part of the Erzgebirge. Lath-shaped plagioclase is typical of the lavas from the eastern Erzgebirge. Apatite is a common component of the groundmass, but can in some cases reach the size of a phenocryst. Tiny flakes of biotite (*c.* 0.02 mm) are found in many samples from both the eastern and the western Erzgebirge.

5.2. Phenocrysts

The most common phenocrysts are clinopyroxene and olivine; amphibole and biotite are of subordinate importance.

5.2.1. Olivine

Olivine is found almost exclusively in lavas from the eastern Erzgebirge and forms the main constituent of the phenocrysts in these rocks. Most of the olivine

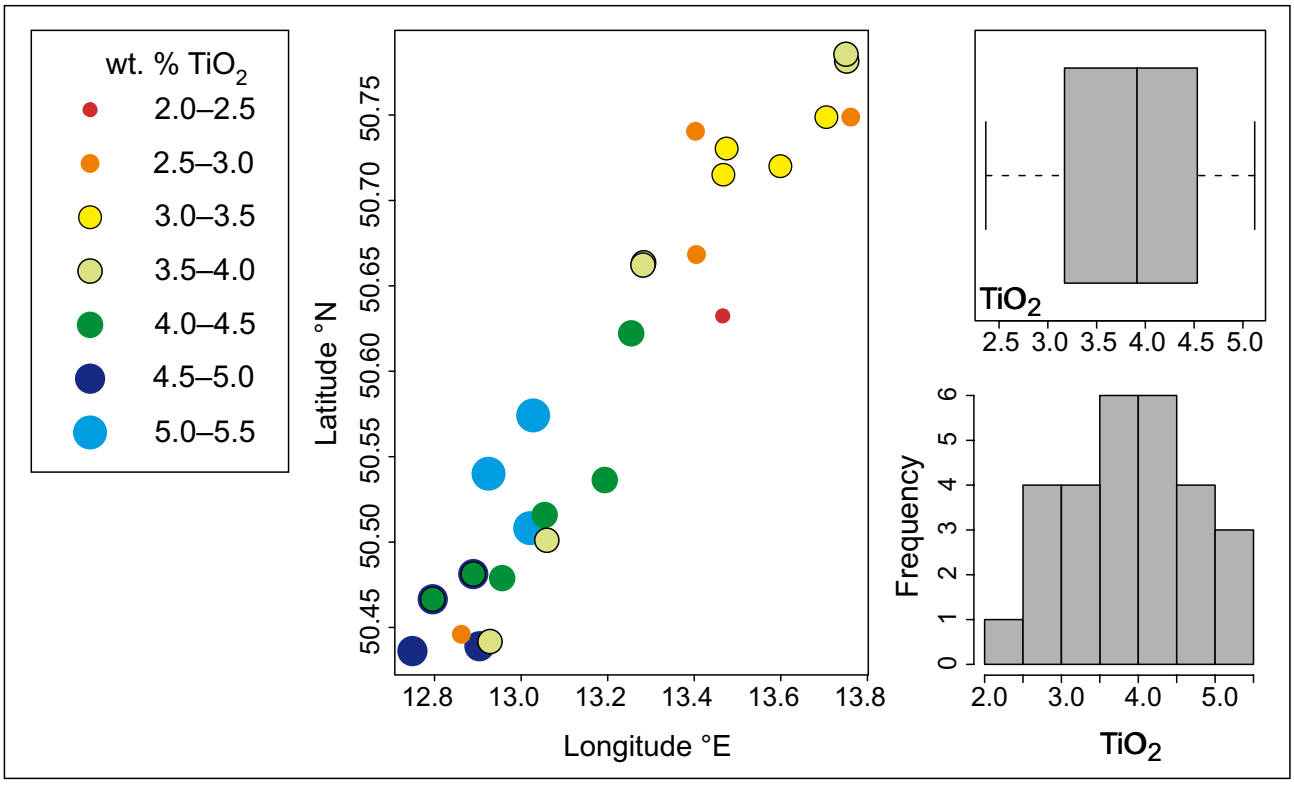

Fig. 4 Regional variation in the TiO_2 contents for the studied basaltic rocks.

crystals are subhedral; skeletal forms are rare. Many show signs of deformation. Visible zoning is restricted to the ultimate rim. Characteristic mineral inclusions are magnetite and brown spinel phases; typical alteration products are serpentine minerals and calcite.

5.2.2. Clinopyroxene

Generally, seven types of clinopyroxene phenocrysts occur in the studied rocks, of which six are shown in Fig. 5. Every type is characterized by the crystallization of an "outermost overgrowth" (**OMG**) of beige–brownish colour showing intense internal oscillatory zoning and sector growth features.

Type 1 Clinopyroxene with a light beige core (**LBC**) of subhedral to anhedral shape. The internal structure of the core shows dissolution features and reaction rims. These cores are always overgrown by the **OMG**.

Type 2 Similar features like Type 1 and additionally a thin fringe around the anhedral central core characterized by a weaker BSE intensity.

Type 3 Typical green-core clinopyroxenes (**GcCpx**) as noted by several authors (Huckenholz 1964, 1965, 1966; Duda and Schmincke 1985) with a size between 0.2 and 2 mm. The central green cores are anhedral and show dissolution features and reaction rims; in very rare cases these cores are zoned. The first overgrowth is by a LBC-type pyroxene followed by the OMG-type. The thickness of the respective zones varies.

Type 4 These form the smallest phenocrysts (0.5 mm) and show internal oscillatory zoning combined with sector zoning features. According to the mineral chemistry (see below) these phenocrysts belong to the **OMG**-type.

Type 5 Anhedral Cr-rich cores characterize this type as demonstrated by EMPA (see below) and show low BSE intensity (**CrCpx**). The first overgrowth is by the **LBC**-type followed by the **OMG**-generation. It is restricted to lavas from the eastern Erzgebirge.

Type 6 Shows the same features as type 5, but is overgrown merely by the **OMG**-type.

Type 7 This forms the so called "giant clinopyroxenes" (**GCpx**), reaching sizes of several centimetres, similar to the **LBC**-type. These megacrysts are overgrown by a very thin rim of the **OMG**-type and restricted to the western Erzgebirge.

5.2.3. Biotite

Biotite phenocrysts, up to 2 cm across, occur in some samples from the western Erzgebirge. These have an anhedral, rounded shape and show signs of bending and kinking. Reaction rims formed at the grain boundaries.

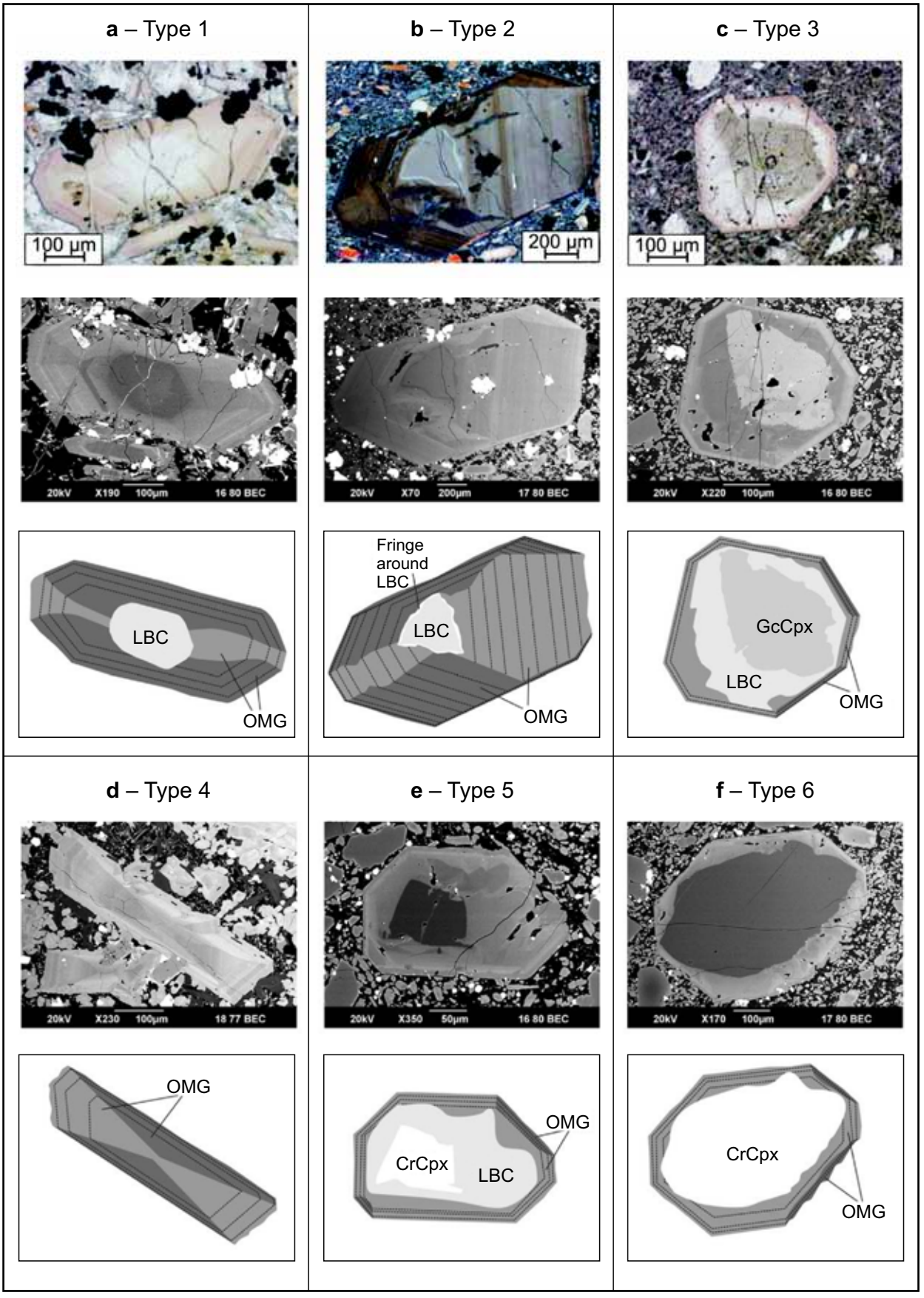
a – Type 1
b – Type 2
c – Type 3
100 µm
200 µm
100 µm
20kV X190 100µm 16 80 BEC
20kV X70 200µm 17 80 BEC
20kV X220 100µm 16 80 BEC
LBC
OMG
Fringe around LBC
LBC
OMG
GcCpx
LBC
OMG
d – Type 4
e – Type 5
f – Type 6
20kV X230 100µm 18 77 BEC
20kV X350 50µm 16 80 BEC
20kV X170 100µm 17 80 BEC
OMG
CrCpx
LBC
OMG
CrCpx
OMG

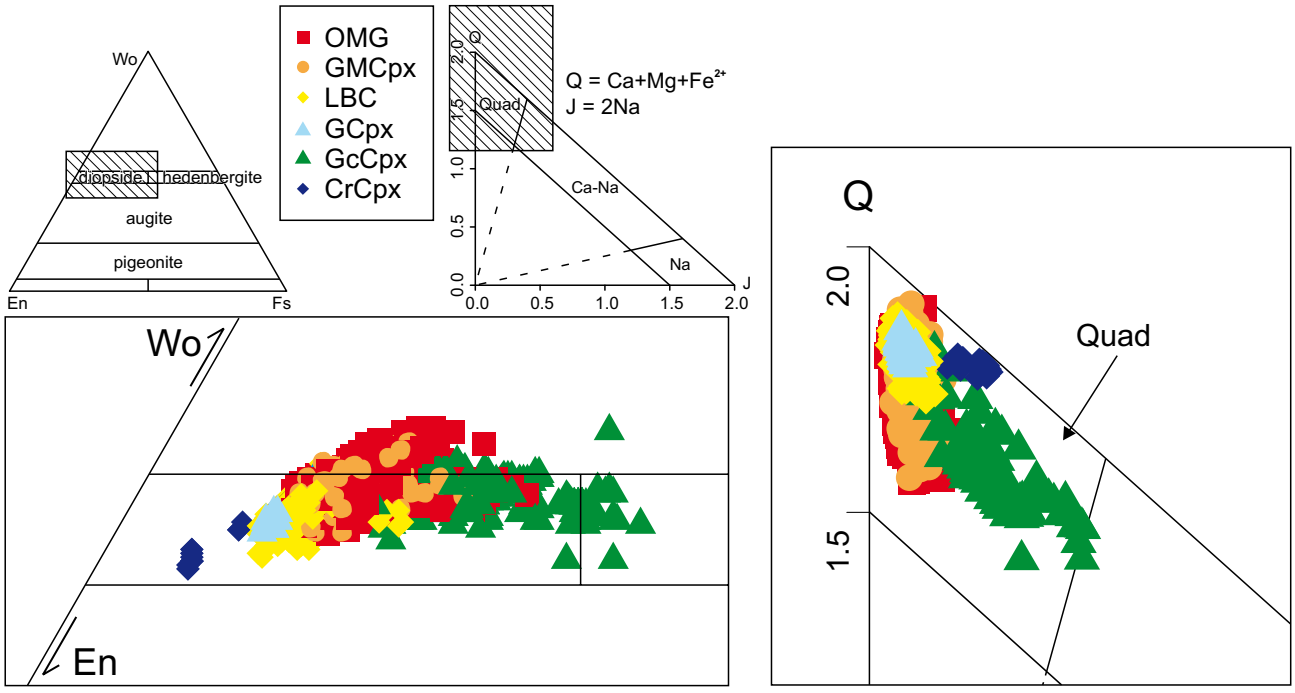

Fig. 6 Plot of analysed clinopyroxenes in classification diagram after Morimoto (1988).

Inclusions of opaque minerals and clinopyroxene are rare. Some of these biotites are intergrown with GCpx.

5.2.4. Amphibole

Two samples carry brownish-green subhedral amphibole crystals. These amphiboles are heterogeneous, but show no clear signs of zoning. Typical are inclusions of opaque minerals.

5.3. Xenoliths and xenocrysts

Many samples contain xenoliths and xenocrysts of crustal (granitoid, gneiss, and sandstone) and mantle origin (spinel lherzolite). The occurrence of mantle-derived material is restricted to samples from the eastern Erzgebirge.

⇦

Fig. 5 Clinopyroxene types in the Erzgebirge basaltic rocks (photomicrographs, back-scattered electron (BSE) images and sketches). **a** – Type 1 clinopyroxene **LBC** of subhedral to anhedral shape. The internal structure of the core shows dissolution features and reaction rims. The **LBC** is overgrown by the **OMG**-type Cpx; **b** – Type 2 resembling the Type 1 but showing additionally a thin fringe around the anhedral **LBC** core characterized by weaker BSE intensity; **c** – Type 3 is a typical green-core clinopyroxene (**GcCpx**). The green core is anhedral and shows effects of resorption and a reaction rim. The first overgrowth is by a **LBC**-type followed by the **OMG**-type clinopyroxene. The thickness of the individual zones varies; **d** – Type 4 forms the smallest phenocrysts and shows internal oscillatory zoning combined with sector growth features. These phenocrysts belong exclusively to the **OMG**-type; **e** – Type 5 characterized by anhedral Cr-rich core (**CrCpx**) with low BSE intensity. The first overgrowth is by the **LBC**-type followed by the **OMG**-generation; **f** – Type 6 shows the same features like Type 5 but is overgrown merely by the **OMG**-type.

6. Crystal chemistry of clinopyroxene

We analyzed 1236 points of the following clinopyroxene types (Tab. 2 and Supp. 4): OMG, groundmass clinopyroxene (**GMCpx**), GCpx, GcCpx, CrCpx and LBC.

In the conventional IMA classification diagram Morimoto (1988) the compositions of the studied clinopyroxenes plot almost exclusively in the diopside field (Fig. 6) and in the "forbidden" field with Wo > 50. In detail, the differences between the individual types are shown in the Mg# versus Si diagram (Fig. 7). The **GcCpx** have distinctive compositions, richest in iron (some crystals were classified as hedenbergite) and with very low Ti (*c.* 0.05 apfu) and relatively high Na (*c.* 0.11 apfu). The **CrCpx** show the highest Mg# (> 87) and Cr_2O_3 contents (up to 0.8 wt. %), and the same enriched Na values like the **GcCpx**. The **LBC** and **GCpx** combine relatively high MgO contents (13–15.1 wt. %) with comparably low Al_2O_3 and FeO concentrations (*c.* 5.5 and 5.7 wt. % respectively). The TiO_2 contents are generally lower than those of the **OMG** and **GMCpx** (*c.* 2 wt. %). Both types show the same crystal chemical features with the highest TiO_2 and Al_2O_3, accompanied by moderate MgO and FeO contents. It has to be stressed that the compositional ranges for individual samples of the given clinopyroxene type may, and often do, overlap significantly with the

Tab. 2 Compilation of electron microprobe analyses and crystal chemical formulae for the individual types of clinopyroxene phenocrysts

East

Type	**OMG** (n = 94)				**GMCpx** (n = 38)				**GcCpx** (n = 46)				**CrCpx** (n = 45)				**LBC** (n = 26)			
	mean	median	min	max	mean	median	min	max	mean	median	min	max	mean	median	min	max	mean	median	min	max
SiO_2	45.34	45.89	38.35	50.42	44.81	44.11	39.60	52.79	46.48	45.51	43.11	52.22	53.85	53.91	52.27	54.52	50.41	50.63	48.70	53.50
TiO_2	3.46	3.21	1.83	5.95	3.15	3.26	0.30	4.99	1.87	1.81	0.71	3.20	0.12	0.07	bd	0.69	1.67	1.74	0.37	2.60
Al_2O_3	8.57	8.49	4.80	13.06	8.33	8.72	0.81	12.34	8.29	9.11	3.02	10.72	2.93	2.77	2.57	4.54	5.37	5.32	3.28	7.01
Cr_2O_3	0.13	0.04	bd	0.81	0.08	0.02	bd	0.68	0.01	0.01	bd	0.07	1.14	1.14	0.90	1.33	0.45	0.45	0.06	0.91
MgO	12.23	12.39	10.01	14.51	12.10	11.83	10.23	14.96	8.86	8.43	6.11	13.03	16.96	17.04	15.26	17.32	14.03	14.06	12.99	15.14
FeO	6.97	7.02	5.39	8.18	7.39	7.44	6.09	8.70	11.81	12.20	8.69	12.94	2.83	2.76	2.60	3.95	5.68	5.69	4.92	6.28
MnO	0.08	0.09	bd	0.17	0.14	0.14	0.09	0.20	0.15	0.08	0.02	0.40	0.03	0.01	bd	0.14	0.10	0.10	0.02	0.22
CaO	23.09	23.09	21.91	23.81	23.22	23.22	22.48	23.96	21.51	21.56	20.32	23.34	20.14	19.79	19.00	22.29	23.43	23.56	22.46	23.89
Na_2O	0.54	0.53	0.34	0.88	0.57	0.56	0.40	0.87	1.49	1.53	0.73	2.48	1.32	1.37	0.94	1.46	0.57	0.54	0.38	0.79
atoms per formula unit Σ = 4																				
Si	1.68	1.69	1.46	1.84	1.67	1.65	1.50	1.96	1.74	1.72	1.66	1.90	1.96	1.96	1.89	1.97	1.83	1.83	1.76	1.92
$Al^{(IV)}$	0.32	0.31	0.16	0.54	0.33	0.35	0.04	0.50	0.26	0.28	0.10	0.34	0.04	0.04	0.03	0.11	0.17	0.17	0.08	0.24
$Fe(III)^{(IV)}$	0.00	0.00	0.00	0.00	0.00	0.00	0.00	0.01	0.00	0.00	0.00	0.00	0.00	0.00	0.00	0.00	0.00	0.00	0.00	0.00
$Al^{(VI)}$	0.05	0.05	0.01	0.09	0.04	0.03	0.00	0.10	0.11	0.13	0.02	0.16	0.08	0.08	0.06	0.10	0.06	0.05	0.02	0.11
$Fe(III)^{(VI)}$	0.11	0.11	0.01	0.19	0.16	0.16	0.06	0.26	0.16	0.16	0.07	0.20	0.02	0.01	0.00	0.04	0.05	0.06	0.01	0.09
Cr	0.00	0.00	0.00	0.02	0.00	0.00	0.00	0.02	0.00	0.00	0.00	0.00	0.03	0.03	0.03	0.04	0.01	0.01	0.00	0.03
Ti	0.10	0.09	0.05	0.17	0.09	0.09	0.01	0.14	0.05	0.05	0.02	0.09	0.00	0.00	0.00	0.02	0.05	0.05	0.01	0.07
Mg	0.67	0.68	0.56	0.80	0.67	0.65	0.58	0.80	0.49	0.47	0.34	0.71	0.92	0.93	0.82	0.94	0.76	0.76	0.71	0.81
Fe(II)	0.10	0.11	0.04	0.16	0.07	0.07	0.00	0.18	0.22	0.22	0.12	0.30	0.07	0.07	0.04	0.09	0.12	0.12	0.08	0.17
Mn	0.00	0.00	0.00	0.01	0.00	0.00	0.00	0.01	0.00	0.00	0.00	0.01	0.00	0.00	0.00	0.00	0.00	0.00	0.00	0.01
Ca	0.92	0.92	0.88	0.94	0.93	0.92	0.90	0.96	0.86	0.86	0.83	0.93	0.78	0.77	0.74	0.86	0.91	0.91	0.87	0.93
Na	0.04	0.04	0.02	0.06	0.04	0.04	0.03	0.06	0.11	0.11	0.05	0.18	0.09	0.10	0.07	0.10	0.04	0.04	0.03	0.06
Mg#	75.62	75.57	69.20	82.75	74.34	74.34	68.87	81.41	56.89	56.11	47.62	72.00	91.44	91.69	87.32	92.10	81.47	81.56	79.01	84.23
IMA end-members Σ = 100 %																				
En	37.24	37.64	32.18	42.70	36.59	36.24	32.78	42.58	28.41	27.81	21.66	37.39	51.35	51.96	45.49	53.07	41.11	41.08	38.91	43.09
Fs	12.10	12.22	9.08	14.80	12.80	12.84	9.90	15.29	21.74	21.99	14.59	24.62	4.84	4.73	4.46	6.76	9.52	9.49	8.13	10.62
Wo	50.66	50.66	47.37	53.36	50.61	50.97	47.52	52.82	49.85	50.00	47.05	54.01	43.81	43.35	41.86	47.76	49.37	49.39	47.68	51.03

Tab. 2 Continued

West

Type	**OMG** (n = 466)				**GMCpx** (n = 97)				**GCpx** (n = 46)				**GcCpx** (n = 71)				**Cr Cpx** (n = 1)	**LBC** (n = 196)			
	mean	median	min	max	mean	median	min	max	mean	median	min	max	mean	median	min	max		mean	median	min	max
SiO_2	44.67	44.76	37.05	52.03	46.42	46.53	40.93	52.30	49.39	49.60	47.76	50.56	45.39	45.27	41.18	48.56	52.38	48.9	48.79	45.43	51.50
TiO_2	4.10	4.02	1.24	8.10	3.70	3.76	1.73	5.97	1.59	1.56	1.31	2.05	2.10	2.11	0.61	4.57	0.97	2.10	2.00	1.17	3.76
Al_2O_3	7.42	7.45	1.06	11.84	6.27	6.43	1.63	10.42	4.32	4.31	3.94	4.80	6.98	7.1	4.18	10.34	2.84	4.63	4.63	3.01	7.54
Cr_2O_3	0.01	0.01	bd	0.37	0.01	bd	bd	0.04	0.03	0.01	bd	0.55	0.01	bd	bd	0.07	0.79	0.05	0.02	bd	0.53
MgO	12.27	12.28	8.8	14.56	12.70	12.8	10.47	14.51	14.41	14.31	13.62	15.49	9.13	9.56	6.79	12.31	16.02	14.16	14.16	12.17	15.72
FeO	6.97	6.93	5.37	9.53	6.87	6.82	5.34	8.46	5.82	5.92	4.87	6.71	11.51	10.93	7.95	14.95	4.16	5.78	5.82	4.64	6.99
MnO	0.09	0.09	0.01	0.26	0.13	0.12	0.05	0.25	0.07	0.07	0.02	0.11	0.35	0.34	0.15	0.59	0.05	0.08	0.08	0.01	0.15
CaO	23.89	23.97	21.99	25.21	23.76	23.85	22.21	24.51	23.61	23.42	22.90	24.30	21.94	22.24	19.94	23.48	23.92	23.80	23.77	22.2	24.83
Na_2O	0.42	0.40	0.22	0.92	0.47	0.44	0.27	0.88	0.44	0.42	0.36	0.59	1.46	1.33	0.61	2.44	0.34	0.42	0.41	0.22	0.71
atoms per formula unit Σ = 4																					
Si	1.67	1.67	1.42	1.95	1.72	1.73	1.54	1.91	1.82	1.83	1.79	1.86	1.73	1.72	1.55	1.83	1.89	1.81	1.80	1.68	1.87
$Al^{(IV)}$	0.32	0.32	0.05	0.52	0.27	0.27	0.07	0.45	0.17	0.17	0.14	0.21	0.27	0.27	0.17	0.42	0.11	0.19	0.19	0.13	0.32
$Fe(III)^{(IV)}$	0.01	0.00	0.00	0.07	0.01	0.00	0.00	0.05	0.00	0.00	0.00	0.01	0.00	0.00	0.00	0.04	0.00	0.01	0.00	0.00	0.05
$Al^{(VI)}$	0.01	0.00	0.00	0.07	0.01	0.00	0.00	0.06	0.01	0.01	0.00	0.04	0.04	0.04	0.00	0.12	0.01	0.01	0.01	0.00	0.06
$Fe(III)^{(VI)}$	0.12	0.13	0.00	0.20	0.10	0.11	0.01	0.18	0.10	0.11	0.04	0.14	0.22	0.22	0.07	0.33	0.04	0.09	0.09	0.00	0.18
Cr	0.00	0.00	0.00	0.01	0.00	0.00	0.00	0.00	0.00	0.00	0.00	0.00	0.00	0.00	0.00	0.00	0.02	0.00	0.00	0.00	0.02
Ti	0.12	0.11	0.03	0.23	0.10	0.10	0.05	0.17	0.04	0.04	0.04	0.06	0.06	0.06	0.02	0.13	0.03	0.06	0.06	0.03	0.10
Mg	0.68	0.68	0.50	0.81	0.70	0.71	0.59	0.79	0.79	0.79	0.75	0.84	0.52	0.54	0.39	0.69	0.86	0.78	0.78	0.67	0.85
Fe(II)	0.08	0.08	0.00	0.23	0.11	0.10	0.03	0.23	0.08	0.07	0.05	0.14	0.15	0.14	0.03	0.27	0.08	0.08	0.08	0.00	0.16
Mn	0.00	0.00	0.00	0.01	0.00	0.00	0.00	0.01	0.00	0.00	0.00	0.00	0.01	0.01	0.00	0.02	0.00	0.00	0.00	0.00	0.00
Ca	0.96	0.96	0.88	1.02	0.94	0.95	0.88	0.99	0.93	0.94	0.91	0.96	0.89	0.91	0.82	0.96	0.93	0.94	0.94	0.88	0.98
Na	0.03	0.03	0.02	0.07	0.03	0.03	0.02	0.06	0.03	0.03	0.03	0.04	0.11	0.10	0.05	0.18	0.02	0.03	0.03	0.02	0.05
Mg#	75.71	75.99	62.21	82.79	76.63	76.80	69.13	82.13	81.51	81.06	78.87	84.69	58.5	60.83	44.74	73.40	87.28	81.33	81.3	75.63	85.42
IMA end-members Σ = 100 %																					
En	36.94	37.02	28.93	42.28	37.81	38.02	33.06	41.48	41.56	41.35	39.68	44.22	28.88	29.74	22.78	36.95	45.03	41.08	41.27	36.13	44.58
Fs	11.26	11.27	6.69	17.80	11.28	11.15	8.48	14.48	9.51	9.70	8.12	10.54	21.14	19.65	12.98	29.13	6.64	9.29	9.32	6.38	11.80
Wo	51.80	51.82	47.90	56.30	50.91	50.96	47.46	54.54	48.93	48.91	47.66	50.86	49.98	50.23	46.85	52.22	48.33	49.64	49.58	46.94	52.10

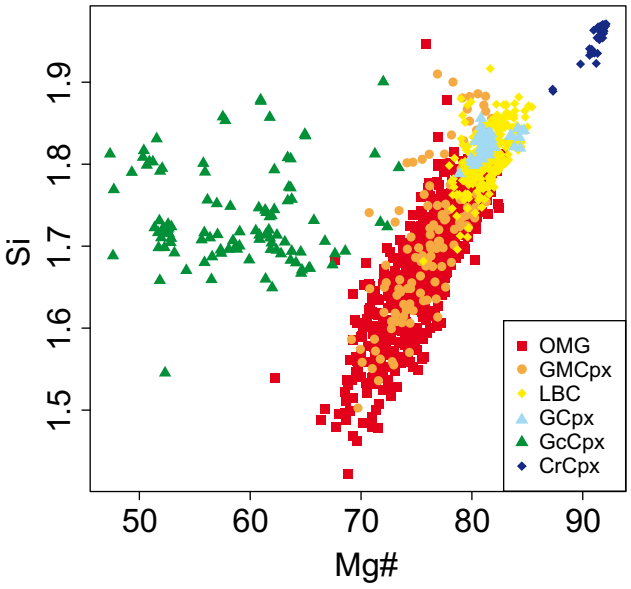

Fig. 7 Binary plot of mg# vs. Si (formula units) for the six clinopyroxene types.

chemical compositions of the other clinopyroxene types. This is shown, for example, in Fig. 8. All groups have invariably wide range of Ca contents varying between 0.8 and 0.99 apfu.

The X-ray concentration maps (Supp. 5) provide a good overview of the microstructural and crystal chemical features of the individual clinopyroxene types.

7. Discussion

The respective chemical and microstructural data for the clinopyroxene phenocrysts bear a witness of multistage, regionally diverse processes leading to the formation of the Ti-rich as well as Ti-poor basalts in the western and eastern Erzgebirge. It is impossible to constrain rates and mass balances with the data available. In particular, we lack high-resolution age determinations of the lavas as well as trace-element and isotope data for the clinopyroxene. Therefore the following hypothesis remains a tentative one. The presumed origin and evolution of the basaltic rocks in the eastern and western Erzgebirge are summarized in Fig. 9.

The first step was the generation of asthenospheric melts (**S1** and **S1***) probably from mantle regions with enhanced activities of H_2O and potassium for the western Erzgebirge, as can be seen from the formation of amphibole and biotite phenocrysts limited to this region.

The chemical characteristics of the **CrCpx** are very similar to data from clinopyroxenes of peridotite xenoliths found in some basalts of the eastern Erzgebirge (A. Renno, unpublished data). Together with xenolithic olivine crystals and mantle-derived peridotite xenoliths, these clinopyroxene crystals were incorporated into the asthenospheric primitive melts **S1** and **S1*** rising rapidly to transient magma chambers or directly to the surface.

The genesis of **GcCpx** is uncertain with several possibilities: (1) crystallization from a geochemically evolved alkaline melt in the upper mantle (Tappe 2004), (2) nucleation from quartz-bearing magmas in a crustal magma chamber (Bédard et al 1988) or (3) formation at the crust–mantle-boundary (Duda and Schmincke 1985). A multistage process involving crystallization from a melt and subsequent reaction with another melt of contrasting composition seems highly probable. We suggest that these **GcCpx** were incorporated as xenocrysts into the first magma batches stored in the lithospheric mantle chambers (**M1A** and **M1b**). They have reacted with the melts **S1** and **S1***, whereby they were overgrown by the **LBC**. Simultaneously, the LBC formed independent, newly grown crystals in these magma chambers. The residence time in the magma chambers associated with the eastern and western parts of the Erzgebirge appears to have been totally different. A short residence demonstrated by the occurrence of mantle-derived xenoliths and xenocrysts in the eastern part (**M1a**) is in contrast with the western part, where long residence times presumably allowed the settling with complete removal of such xenoliths and xenocrysts as well as the formation of the **GCpx** in **M1b**.

The fractionated melts **S2a** and **S2b** rose to the shallower magma chambers **M2a** and **M2b**, situated probably at a crustal level. These areas appear to be locations of intense magma mixing of the melts **S2a** or **S2b** with Ti-rich melts **S3a** and **S3b**. The existence of these Ti-rich melts in both parts of the Erzgebirge is demonstrated by the crystallization of the chemically mutually identical **OMG** and **GMCpx** phases. The **LBC**, **GCpx**, **GcCpx**, biotite phenocrysts and the mantle-derived olivine xenocrysts all reacted with the newly formed melt. The existence of schlieren-like heterogeneities in the groundmass of some of the lavas suggests that these mixing processes lasted for considerable time and were themselves multistage in character. The geochemical differences among the basaltic rocks demonstrate the significantly lower involvement of the hypothetical Ti-rich melt **S3a** in these mixing processes in the east.

The ultimate origin of the Ti-rich melts **S3a** and **S3b** remains unexplained. Eclogite-derived melts appear as a viable possibility. Melting experiments e.g., by Klemme et al. (2002) showed that the partial melting of eclogite at temperatures similar to, or exceeding 1300 °C and a pressure of 3 GPa could yield melts enriched in Ti and Na. Eclogites derived from subducted oceanic crust

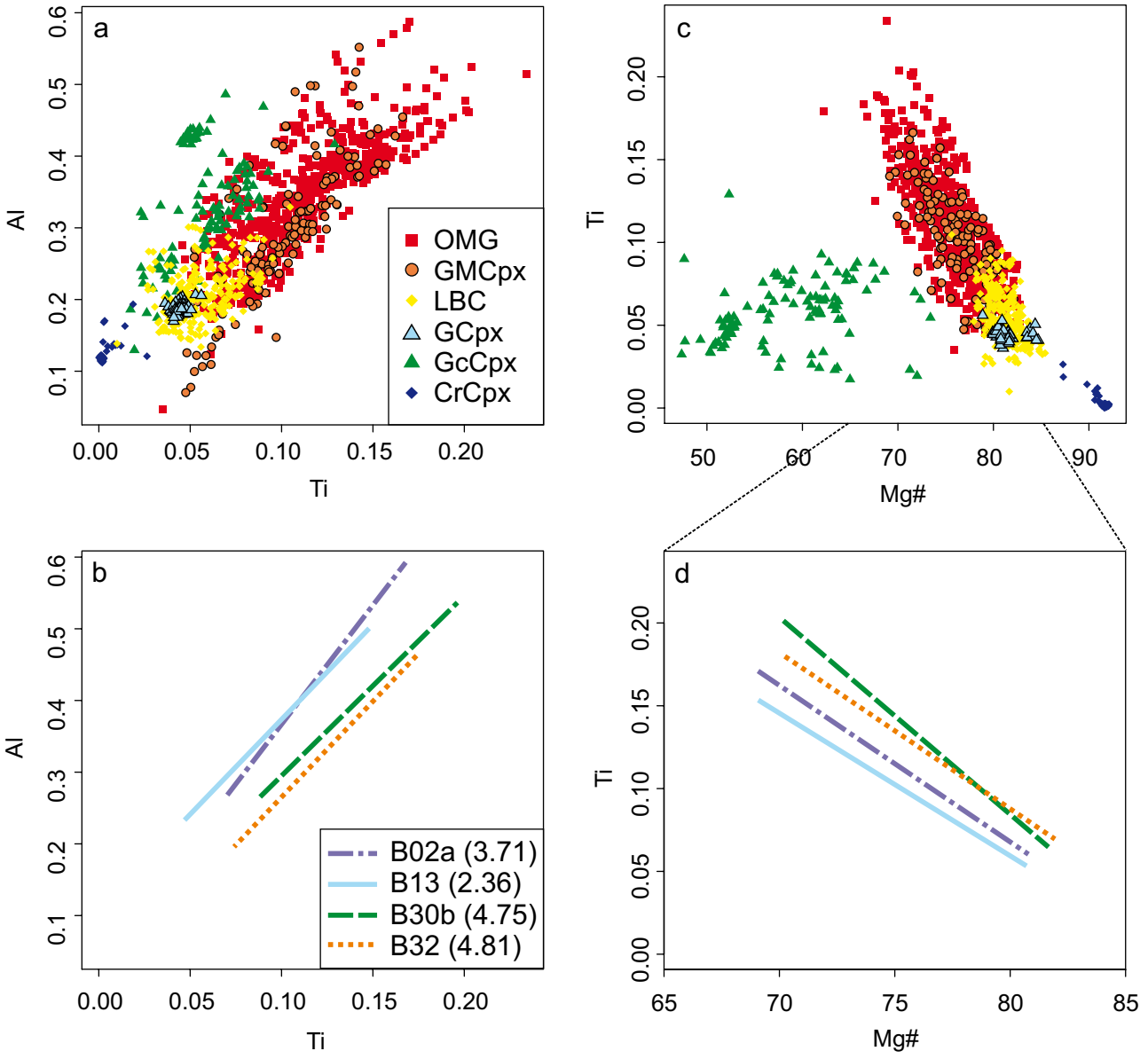

Fig. 8a – Ti vs. Al (formula units) diagram of the individual clinopyroxene types; **b** – Ti vs. Al (formula units) diagram showing the variability of data for the **OMG**-type Cpx using four selected samples as an example (whole-rock TiO_2 contents in parentheses); **c** – Mg# vs. Ti (formula units) diagram of the individual clinopyroxene types; **d** – Mg# vs. Ti (formula units) diagram showing the range of data for the **OMG**-type Cpx using four selected samples as an example (whole-rock TiO_2 contents in parentheses).

represent an important component of the Saxothuringian lithosphere, as demonstrated by the common presence of exhumed eclogites in the upper crust (e.g., Schmädicke et al. 1992; Konopásek and Schulmann 2005). The mixing of these very hot melts with the **S1** and **S2** magmas in the shallow magma chambers should have triggered the resorption of the **GcCpx** and the **LCB** as well as the assimilation of continental crustal material. Indeed, the crustal contamination (biotite flakes and crustal xenoliths) was likely coeval with the mixing in the magma chambers **M2a** and **M2b**.

8. Conclusions

The synopsis of the petrographic, microstructural and chemical features of several types of clinopyroxenes from cenozoic basaltic rocks in the eastern and the western Erzgebirge demonstrated that the origin of the parental Ti-poor and Ti-rich basaltic melts was a multistage process. At least three different melts were involved in fractionation, assimilation and magma-mixing in two magma chamber systems at different depths, in the lithospheric mantle and in the crust. The regional dichotomy

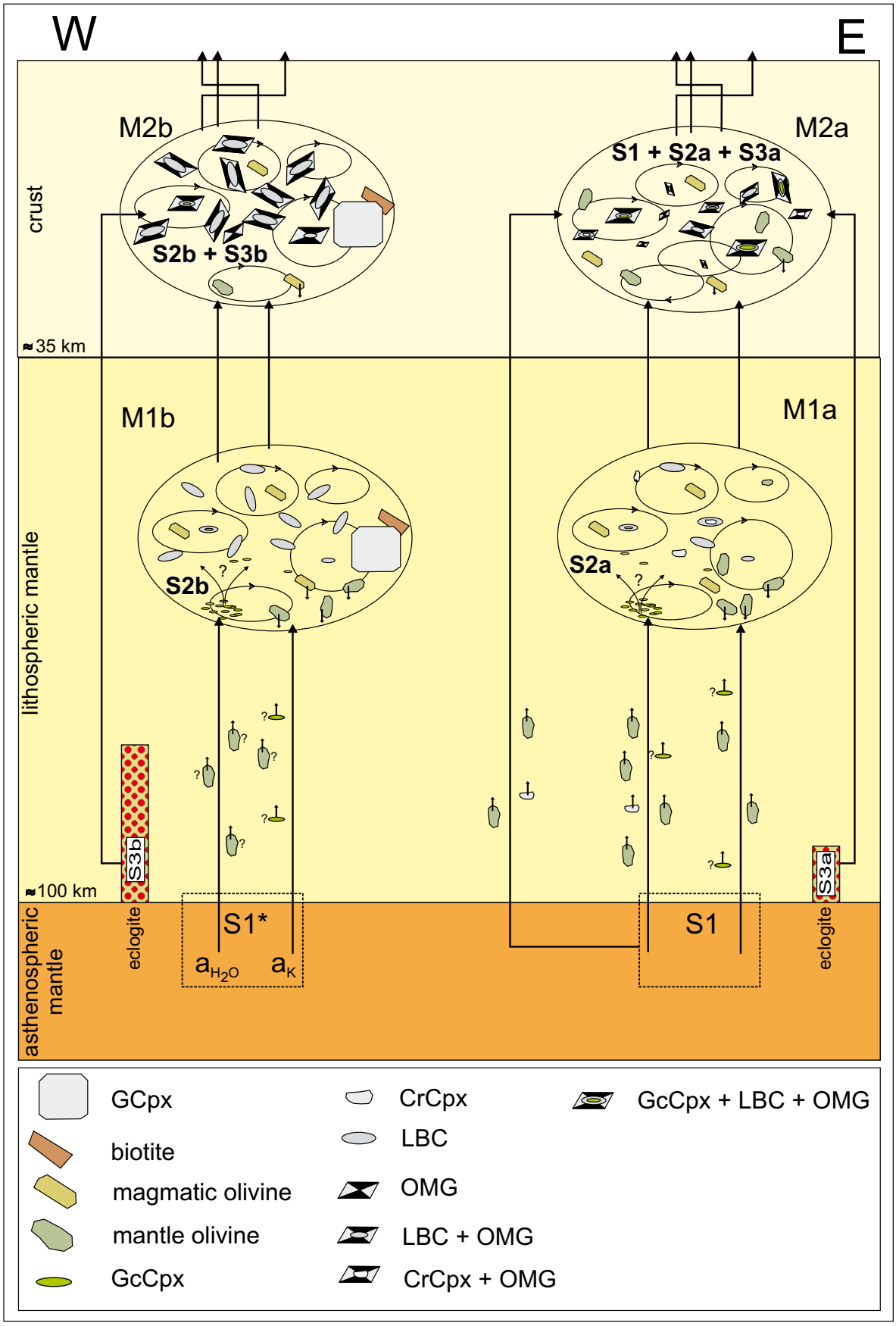
W
E
M2b
M2a
S1 + S2a + S3a
S2b + S3b
crust
≈35 km
M1b
M1a
S2b
S2a
lithospheric mantle
≈100 km
S3b
S3a
eclogite
eclogite
S1*
S1
a_{H_2O}
a_K
asthenospheric mantle
GCpx
biotite
magmatic olivine
mantle olivine
GcCpx
CrCpx
LBC
OMG
LBC + OMG
CrCpx + OMG
GcCpx + LBC + OMG

between the eastern and western Erzgebirge basaltic rocks is interpreted by differences in the residence time of the parental magmas in the transient magma chambers, as well as variable mixing with hot Ti-rich melts, possibly derived from an eclogitic source.

Acknowledgements. We gratefully acknowledge the help of A. Pleßow, T. Tschöpe, K. Treptow, and E. Rüdiger with the analytical work. We express our thanks to Jaromír Ulrych and Stanislav Vrána for their careful reviews and to the guest editor Vladislav Rapprich for the subtle and stringent editorial handling of the manuscript. Matthew Huber improved the English style and grammar. This work was funded by the DFG through grant Ha 2568/10-1.

Electronic supplementary material. The GPS coordinates and a map of the sampling sites, detailed petrographic features for the analysed basaltic rocks, the complete set of variation diagrams for the Erzgebirge basaltic rocks including a compilation of the regional variation in major elements and mg#, all mineral compositional data for clinopyroxene and X-ray concentration maps for several typical clinopyroxene crystals are available online at the Journal web site *(http://dx.doi.org/10.3190/jgeosci.077)*.

References

Babuška V, Plomerová J (1992) The lithosphere in central Europe – seismological and petrological aspects. Tectonophysics 207: 141–163

Babuška V, Plomerová J (2010) Mantle lithosphere control of crustal tectonics and magmatism of the western Ohře (Eger) Rift. J Geosci 55: 171–186

Babuška V, Plomerová J, Fischer T (2007) Intraplate seismicity in the western Bohemian Massif (central Europe): a possible correlation with a paleoplate junction. J Geodyn 44: 149–159

Bédard JH, Francis DM, Ludden J (1988) Petrology and pyroxene chemistry of Monteregian dykes; the origin of concentric zoning and green cores in clinopyroxenes from alkali basalts and lamprophyres. Can J Earth Sci 25: 2041–2058

⇦

Fig. 9 Tentative model for the formation of the basaltic rocks in the western (W, labelled by 'a') and eastern (E, labelled by 'b') Erzgebirge, respectively. **S1** = primary asthenospheric melt (E Erzgebirge); **S1*** = primary asthenospheric melt with higher a_{H2O} and a_K (W Erzgebirge); **S2a, S2b** = fractionated melts from the first magma chamber system in the lithospheric mantle; **S3a, S3b** = eclogite-derived melts; **M1a, M1b** = first magma chamber in the lithospheric mantle; **M2a, M2b** = second (crustal) magma chamber systems.

Bogaard PJF, Wörner G (2003) Petrogenesis of basanitic to tholeiitic volcanic rocks from the Miocene Vogelsberg, Central Germany. J Petrol 44: 569–602

Duda A, Schmincke H–U (1985) Polybaric differentiation of alkali basaltic magmas: evidence from green-core clinopyroxenes (Eifel, FRG). Contrib Mineral Petrol 91: 340–353

Duncan AR (1987) The Karoo Igneous Province – a problem area for inferring tectonic setting from basalt geochemistry. J Volcanol Geotherm Res 32: 13–34

Dupuy C, Marsh J, Dostal J, Michard A, Testa S (1988) Asthenospheric and lithospheric sources for Mesozoic dolerites from Liberia (Africa): trace element and isotopic evidence. Earth Planet Sci Lett 87: 100–110

Essawy MA, El-Metwally AA (1999) Petrogenesis of a high TiO_2 mafic dyke swarm from southwest Sinai. J Afr Earth Sci 29: 551–565

Fodor RV (1987) Low- and high-TiO_2 flood basalts of southern Brazil: origin from picritic parentage and a common mantle source. Earth Planet Sci Lett 84: 423–430

Gibson SA, Thompson RN, Dickin AP, Leonardos OH (1995) High-Ti and low-Ti mafic potassic magmas: Key to plume-lithosphere interactions and continental flood-basalt genesis. Earth Planet Sci Lett 136: 149–165

Goes S, Loohuis JJP, Wortel MJR, Govers R (2000) The effect of plate stresses and shallow mantle temperatures on tectonics of northwestern Europe. Global Planet Change 27: 23–38

Haase KM, Renno AD (2008) Variation of magma generation and mantle sources during continental rifting observed in Cenozoic lavas from the Eger Rift, Central Europe. Chem Geol 257: 192–202

Hrubcová P, Środa P, Špičák A, Guterch A, Grad M, Keller GR, Brueckl E, Thybo H (2005) Crustal and uppermost mantle structure of the Bohemian Massif based on CELEBRATION 2000 data. J Geophys Res B Solid Earth 110: 1–21, DOI: 10.1029/2004JB003080

Huckenholz HG (1964) Der petrogenetische Werdegang der Klinopyroxene in den tertiären Vulkaniten der Hocheifel I. Die Klinopyroxene der Alkaliolivinbasalt–Trachyt–Assoziation. Contrib Mineral Petrol 11: 138–195

Huckenholz HG (1965) Der petrogenetische Werdegang der Klinopyroxene in den tertiären Vulkaniten der Hocheifel II. Die Klinopyroxene der Basanitoide. Contrib Mineral Petrol 11: 415–448

Huckenholz HG (1966) Der petrogenetische Werdegang der Klinopyroxene in den tertiären Vulkaniten der Hocheifel. Contrib Mineral Petrol 12: 73–95

Jama Aden A, Frizzo P (1996) Geochemistry and origin of low and high TiO_2 mafic rocks in the Barkasan Complex: a comparison with common Neoproterozoic gabbros of northern Somali crystalline basement. J Afr Earth Sci 22: 43–54

Janoušek V, Farrow CM, Erban V (2006) Interpretation of whole-rock geochemical data in igneous geochemistry: introducing Geochemical Data Toolkit (GCDkit). J Petrol 47: 1255–1259

Jung S, Hoernes S (2000) The major- and trace-element and isotopic (Sr, Nd, O) geochemistry of Cenozoic alkaline rift-type volcanic rock from the Rhön area (central Germany): petrology, mantle source characteristics and implications for asthenosphere–lithosphere interactions. J Volcanol Geotherm Res 99: 27–53

Kaiser G, Pilot J (1986) Weitere K–Ar-Datierungen an jungen Vulkaniten. Z geol Wiss 14: 121–124

Katzir Y, Litvinovsky B, Eyal M, Zanvilevich A, Vapnik Y (2006) Four successive episodes of Late Pan-African dikes in the central Elat area, southern Israel. Isr J Earth Sci 55: 69–93

Klemme S, Blundy JD, Wood BJ (2002) Experimental constraints on major and trace element partitioning during partial melting of eclogite. Geochim Cosmochim Acta 66: 3109–3123

Konopásek J, Schulmann K (2005) Contrasting Early Carboniferous field geotherms: evidence for accretion of a thickened orogenic root and subducted Saxothuringian crust (Central European Variscides). J Geol Soc, London 162: 463–470

Le Bas MJ (1989) Nephelinitic and basanitic rocks. J Petrol 30: 1299–1312

Le Bas MJ, Le Maitre RW, Streckeisen A, Zanettin B, IUGS Subcomission on the Systematics of Igneous Rocks (1986) A chemical classification of volcanic rocks based on the total alkali–silica diagram. J Petrol 27: 745–750

Le Maitre RW, Streckeisen A, Zanettin B, Le Bas MJ, Bonin B, Bateman P (2005) Igneous Rocks: A Classification and Glossary of Terms: Recommendations of the International Union of Geological Sciences Subcommission on the Systematics of Igneous Rocks. Cambridge University Press, Cambridge, pp 1–252

Malkovský M (1987) The Mesozoic and Tertiary basins of the Bohemian Massif and their evolution. Tectonophysics 137: 31–42

Middlemost EAK (1994) Naming materials in the magma/igneous rock system. Earth Sci Rev 37: 215–224

Mlčoch B, Konopásek J (2010) Pre-Late Carboniferous geology along the contact of the Saxothuringian and Teplá–Barrandian zones in the area covered by younger sediments and volcanics (western Bohemian Massif, Czech Republic). J Geosci 55: 81–94

Morimoto N (1988) Nomenclature of pyroxenes. Bull Minéral 111: 535–550

Murphy JB (1988) Late Precambrian to Late Devonian mafic magmatism in the Antigonish Highlands of Nova Scotia: multistage melting of a hydrated mantle. Can J Earth Sci 25: 473–485

Niese S, Pfeiffer L, Gleisberg GB (1995) Geochemie sächsischer Tertiärmagmatite. Z geol Wiss 23: 317–330

Papike JJ, Vaniman DT (1978) The Lunar Mare Basalt suite. Geophys Res Lett 5: 433–436

Papike JJ, Hodges FN, Bence AE, Cameron M, Rhodes JM (1976) Mare basalts: crystal chemistry, mineralogy, and petrology. Rev Geophys 14: 475–540

Pfeiffer L (1978) Beitrag zur Petrochemie der sächsischen Tertiärvulkanite. Freiberg Forsch H C333: 1–164

Pik R, Deniel C, Coulon C, Yirgu G, Hofmann C, Ayalew D (1998) The northwestern Ethiopian Plateau flood basalts: classification and spatial distribution of magma types. J Volcanol Geotherm Res 81: 91–111

Pik R, Marty B, Hilton DR (2006) How many mantle plumes in Africa? The geochemical point of view. Chem Geol 226: 100–114

Pilot J, Pfeiffer L, Rösler HJ, Schlichting M, Kaiser G (1984) Zur genetischen Problematik der tertiären Vulkanite von der Lausitz und des Erzgebirges auf Grund von Strontiumisotopenverhältnissen, Rb–Sr- und K–Ar-Altern. Freiberg Forsch H C389: 84–92

Plomerová J, Achauer U, Babuška V, Vecsey L (2007) Upper mantle beneath the Eger Rift (Central Europe): plume or asthenosphere upwelling? Geophys J Int 169: 675–682

Prodehl C, Müller S, Haak V (1995) The European Cenozoic rift system. In: Olsen KH (ed) Continental Rifts: Evolution, Structure, Tectonics. Elsevier, Amsterdam, pp 133–212

Rapprich V (2005) Compositional variation of clinopyroxenes of basaltic, essexitic and tephriphonolitic rocks from the Doupovské hory Volcanic Complex, NW Bohemia. J Czech Geol Soc 50: 119–132

Rönick R (2010) Geochemisch-petrologische Untersuchungen an Ti-reichen Basalten des Erzgebirges. Unpublished Diploma thesis, TU Bergakademie Freiberg – Institut für Geologie, pp 1–124

Schmädicke E, Okrusch M, Schmidt W (1992) Eclogite-facies rocks in the Saxonian Erzgebirge, Germany: high pressure metamorphism under contrasting P–T conditions. Contrib Mineral Petrol 110: 226–241

Shrbený O (1995) Chemical composition of young volcanites of the Czech Republic. Czech Geol Survey Spec Pap 4: 1–53

Tappe S (2004) Mesozoic mafic alkaline magmatism of southern Scandinavia. Contrib Mineral Petrol 148: 312–334

Todt W, Lippolt HJ (1975) K–Ar Altersbestimmungen an Vulkaniten bekannter paläomagnetischer Feldrichtung II Sachsen. J Geophysics 41: 641–650

Ulrych J (1986) Clinopyroxenes in the Cenozoic volcanics of the České středohoří Mts.: a review. Acta Univ Carol, Geol 1986: 117–131

Ulrych J, Pivec E, Rutšek J, Povondra P (1990) Olivines–monticellites and clinopyroxenes in melilitic rocks,

Ploučnice River region, Czechoslovakia. Acta Univ Carol, Geol 1990: 141–164

Ulrych J, Svobodová J, Balogh K (2002) The source of Cenozoic volcanism in the České středohoří Mts., Bohemian Massif. Neu Jb Mineral, Abh 177: 133–162

Ulrych J, Lloyd FE, Balogh K, Hegner E, Langrová A, Lang M, Novák JK, Řanda Z (2005) Petrogenesis of alkali pyroxenite and ijolite xenoliths from the Tertiary Loučná–Oberwiesenthal Volcanic Centre, Bohemian Massif in the light of new mineralogical, geochemical, and isotopic data. Neu Jb Mineral, Abh 182: 57–79